Orientation of spheroidal fullerenes inside carbon nanotubes with potential applications as memory devices in nano-computing

2008 J. Phys. A: Math. Theor. 41 235209

(http://iopscience.iop.org/1751-8121/41/23/235209)

IOP PUBLISHING JOURNAL OF PHYSICS A: MATHEMATICAL AND THEORETICAL

J. Phys. A: Math. Theor. **41** (2008) 235209 (27pp) doi:10.1088/1751-8113/41/23/235209

Orientation of spheroidal fullerenes inside carbon nanotubes with potential applications as memory devices in nano-computing

Barry J Cox, Ngamta Thamwattana and James M Hill

Nanomechanics Group, School of Mathematics and Applied Statistics, University of Wollongong, Wollongong, NSW 2522, Australia

E-mail: barryc@uow.edu.au

Received 7 March 2008, in final form 24 April 2008
Published 21 May 2008
Online at stacks.iop.org/JPhysA/41/235209

Abstract

A spheroid is an ellipsoid for which two of the axes are equal, and here the interaction between spheroidal fullerenes and carbon nanotubes is modeled using the Lennard–Jones potential and the continuum approximation. The resulting surface integrals are evaluated analytically for a number of configurations, including lying and standing as well as spheroids with an arbitrary tilt angle, and centered on the nanotube axis. Analytical expressions for off-axis spheroids in all three orientations are also given, and the findings are shown to agree well with previously published work. However, the major contribution of this work is the derivation of new exact analytical formulae to calculate the van der Waals interaction energy for these configurations, and in particular the results for the tilting and off-axis configurations which are far more general than those which have appeared in the literature previously. From these exact expressions, five primary regimes are identified: lying on-axis, tilting on-axis, standing on-axis, standing off-axis and finally lying off-axis. Also identified in this study is a precisely prescribed radius, for the transition between regimes four and five, for which two equally energetically favorable orientations exist and for which these two configurations are separated by a known energy barrier. The notion arises that such configurations may be exploited for nano-scaled memory devices used in nano-computing.

PACS number: 61.48.+c

1. Introduction

The discovery of carbon nanostructures has led to the possible creation of many nanodevices. Carbon nanotubes in particular have attracted much attention due to their mechanical,

electronic and energetics properties. One further aspect of carbon nanotubes, which is of particular interest, is their accessible internal storage capacity via their open ends which can be filled with other molecular structures. In [1], it was first observed that hollow nanotubes may be filled with C_{60} fullerene molecules, the resulting structures being usually referred to as nanopeapods. While earlier attention is given to C_{60} molecules inside the nanotubes [2], Hodak and Girifalco [3–5], report different types of fullerene forming nanopeapods, including C_{70}, C_{78} and C_{80} (see, for example, [6, 7]). As mentioned in [8, 9], nanopeapods possess potential applications as superconducting nanowires. The superiority of using nanopeapods instead of an empty carbon nanotube to create a superconducting nanowire is because the charge can travel not only along the tube wall, but also along the chain of fullerenes inside the nanotube. However, Okada *et al* [10] find that the C_{60} at (10,10) peapod is a metal with multi-carriers, each of which distributes either along the nanotube or along the chain of fullerenes C_{60}, while the C_{60} at (9,9) peapod does not exhibit this character. We also note from Okada *et al* [2, 10] that the incorporation of a C_{60} molecule into a (10,10) nanotube is energetically favorable, whereas this is not the case for (9,9) nanotubes due to large structural deformation of both the tubes and the fullerenes. These results lead to the studies of energetics and electronic structures of nanopeapods by Otani *et al* [11] and Okada *et al* [10] where a comparison of the energies of the peapods which comprise fullerenes encapsulated in zigzag and armchair nanotubes is made and they find that both energies exhibit qualitatively the same characteristics. Their findings indicate that the space in the tube, which is the inter-wall spacing between the encapsulated fullerene and the nanotube, is the crucial factor for determining the energetics of nanopeapods and the stability of the nanopeapod system, rather than the metallic or semiconducting characteristics or atomic arrangements of the tube. Consequently, Otani *et al* [11] point out that the determination of the energetics stability of various carbon nanopeapods can be carried out solely by consideration of the space issue. For C_{60}-peapods, the inter-wall spacing between the fullerene and the nanotube depends only on the radii of the tube and the fullerene. However, for peapods with ellipsoidal fullerenes, such as C_{70} and C_{80} the inter-wall spacing is also dependent on the orientation of the fullerenes. Evidently, due to their non-spherical structure, spheroidal fullerenes can pose different orientations inside the nanotubes, unlike spherical fullerenes C_{60}. This also leads to an advantage that spheroidal fullerene peapods have over the C_{60}-peapods, which is a capacity to control the electronic properties of the system by simply controlling the orientations of the fullerenes [12].

In previous work [13], the present authors examined the energetic issues of spheroidal fullerenes being accepted into carbon nanotubes, assuming that the spheroid is lying on the nanotube axis. In the present paper, we extend this work by specifically addressing the issue of the orientation of the spheroidal fullerenes C_{70} and C_{80} inside a single-walled carbon nanotube. Since the chirality of the carbon nanotube does not affect either the electronic structure and energetic properties of the nanopeapods [11] or the orientation of the spheroidal fullerenes [14], we adopt the continuum approach for which we assume that carbon atoms are uniformly distributed over the surface of the molecules. Thus, instead of summing the interaction between each atom pair, the total interaction potential energy can be obtained by performing surface integrals of a potential energy, which in this paper we adopt the classical six-twelve Lennard–Jones potential. To predict the orientations of C_{70} molecules in carbon nanotubes, the continuum approach has also been previously employed by Verberck and Michel [14] and Chorro *et al* [15]. While here we assume continuity of surface density for both the nanotube and fullerene, in [14], only the carbon nanotube is modeled as a continuum, while the fullerene is assumed to retain its discrete atomic structure. Similarly, Chorro *et al* [15] also model the nanotube as a cylinder with uniform atomic surface density. However, the fullerene is described as generated by nine circular slices of the same linear density. We note that while

the Lennard–Jones potential is used in the present paper and in Chorro *et al* [15], Verberck and Michel [14] use the Born–Mayer–van der Waals potential. Further, we note that a number of techniques, including electron diffraction studies [15–17] and local density approximations [6, 10–12] have been employed in order to predict the orientation of the C_{70} molecules inside carbon nanotubes.

As mentioned in [6, 11, 12, 15, 17], in a thin nanotube with approximate diameter of 13.6 Å, the fullerene C_{70} adopts a lying configuration, which is when the molecule's long (or polar) axis lays parallel to the tube central axis, and when the nanotube becomes larger the fullerene adopts the standing configuration for which the molecule's polar axis lays perpendicular to the tube axis. For those tube sizes in between the two that the molecule adopts the lying and standing arrangements, it is suggested that the molecule adopts an intermediate state for which the angle ψ between the long axis of the fullerene and the tube axis is between zero and $\pi/2$ radians. However, in these studies [6, 11, 12, 15, 17] the center of the spheroidal fullerene is assumed to be located on the tube central axis. While this assumption may be valid for a small nanotube, for a large nanotube the fullerene tends to be offset from the tube axis and becomes closer to one side of the nanotube wall. For example, as shown in [18, 19] in a (10,10) nanotube, the center of the C_{60} fullerene is on the tube axis, whereas in a (16,16) nanotube the C_{60} molecule dislodges from the tube axis by 4.314 Å. Thus, we might expect the spheroidal fullerenes to be offset from the tube central axis in a large nanotube. Although Verberck and Michel [14] allow the center of the C_{70} molecule to be off-axis, they consider only the cases when the angle $\psi = 0$ and $\pi/2$, which corresponds to the lying or standing arrangements, respectively. In this paper, allowing the molecule to be off-axis we do not make this restriction of fixing the angle ψ for the offset molecule, and consequently the orientations of the spheroidal fullerenes obtained here are the true minimum energy configuration of the fullerenes inside the nanotubes.

In the following section, we describe the method used to calculate the results contained in this paper and then in section 3 we present the results for spheroidal fullerenes interacting with flat graphene, and then carbon nanotubes, both when the spheroid is centered on the nanotube axis and when the spheroid is offset from the nanotube axis by some distance ε. In section 4, we then summarize these results and provide a description of five regimes which exist depending on the particular fullerene and the radius of the nanotube in question. Ten appendices are included in which the full mathematical derivations of the analytical expressions used in these calculations are presented. In appendix A an expression is derived for a point interacting with a graphitic plane, which is followed by appendices B and C which extend this result for spheroidal fullerenes in the lying and standing orientations, respectively. Similarly, appendix D provides a general result for a point and a carbon nanotube, and this result is extended to on-axis lying, standing and tilting fullerenes in appendices E, F and G, respectively. Finally, appendices H, I and J deal with analytical expressions for lying, standing and tilting fullerenes which are not centered on the nanotube axis. We comment that the extensive computations undertaken here are facilitated by the use of the explicit formulae which are derived in the appendices. To generate the equivalent data using either molecular dynamics simulation or other computational schemes would require considerably more computational effort than that involved here.

2. Method

In this paper, we calculate the interaction energy of the fullerenes C_{70} and C_{80} using the various expressions given in the appendices of this paper. This is done first for those systems when the fullerene is interacting with graphene, because this interaction energy represents a limiting

Table 1. Constants used in the model.

Mean surface density for graphene	$\eta_g = 0.3812$ Å^{-2}
C_{70} equatorial semi-axis length	$b = 3.59$ Å
C_{70} polar semi-axis length	$c = 4.17$ Å
Mean surface density for fullerene C_{70}	$\eta_{70} = 0.3896$ Å^{-2}
C_{80} equatorial semi-axis length	$b = 3.58$ Å
C_{80} polar semi-axis length	$c = 4.73$ Å
Mean surface density for fullerene C_{80}	$\eta_{80} = 0.4072$ Å^{-2}
Attractive constant	$A = 17.4$ eV $\times$ Å^6
Repulsive constant	$B = 29 \times 10^3$ eV $\times$ Å^{12}

case of the interaction with a carbon nanotube in the limit of a very large radius. Following this we investigate those cases when the fullerene is fully encapsulated within a nanotube. First, in the case when the fullerene is centrally located on the axis of the nanotube, and then we examine those cases with the fullerene free to move off the nanotube axis.

Throughout this paper, we use those values for the attractive and repulsive constants as given by Girifalco *et al* [20] and the dimensions of the C_{70} and C_{80} fullerenes are taken from Nakao *et al* [21], where we choose the C_{80} isomer with D_{5d} symmetry since it possesses the most spheroidal shape. We comment that the analysis presented here is valid for any spheroidal fullerene and not limited to these two molecules. The values of these constants are given in table 1. The numerical evaluation is performed with MAPLE using the function to evaluate the usual hypergeometric functions. The evaluation of the Appell's functions is facilitated by using the series expansion (30) contained in Burchnall and Chaundy [22].

3. Numerical results

3.1. Interaction of spheroidal fullerene with flat graphene

In this section, we investigate the minimum energy configuration of spheroidal fullerenes with a flat plane of graphene. We utilize the expressions derived in appendices B and C to determine the energy which the fullerene interacts with a sheet of graphene and this calculation serves two purposes. First, this expression can be used to determine the interaction energy for fullerenes and graphene and by an appropriate sum, graphite. Second, the primary purpose of this paper is to determine those configurations of fullerenes in carbon nanotubes, and the limit as the tube radius goes to infinity is that of a flat graphene plane.

In figure 1, we show the interaction energies for C_{70} and C_{80} fullerenes and a single graphene sheet. These are calculated using the expressions for E_{gl} given in equations (B.1) and (B.2) and E_{gs} given in equations (C.1) and (C.4). We see that in both cases the standing orientation is energetically favored at a distance but as the fullerene approaches the graphene sheet, the lying configuration begins to take over and the global minimum occurs for the lying configuration. For the C_{70} this value is -0.849 eV which occurs at a distance of 6.56 Å. In the case of the C_{80} fullerene this global minimum has a value of -0.980 eV which occurs at a distance of 6.55 Å. If we consider just the standing orientation then the C_{70} fullerene obtains a global minimum energy of -0.717 eV at an offset distance of 7.11 Å, and for the C_{80}, this minimum value is -0.709 eV which is present for an offset distance of 7.66 Å.

3.2. Interaction of an axially centered spheroidal fullerene with a carbon nanotube

In this section, we investigate the various orientations of a single spheroidal fullerene inside an infinite carbon nanotube with the center of the spheroid lying on the axis of the nanotube.

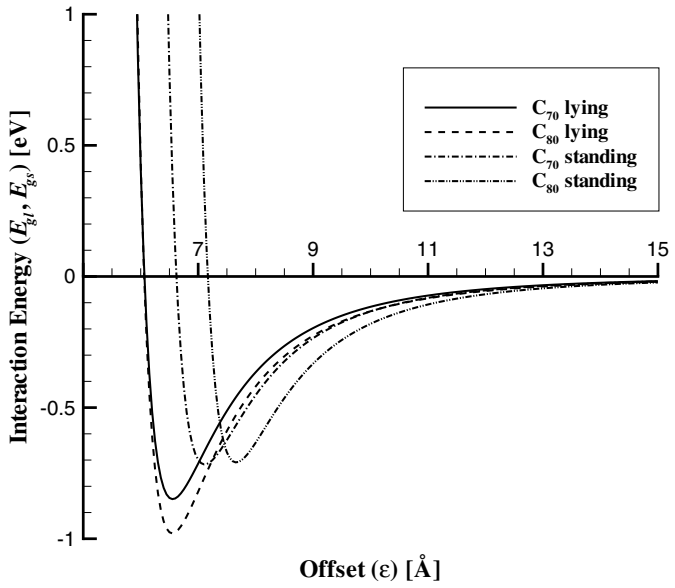

Figure 1. Interaction energy between graphene and fullerenes, both lying in E_{gl} and standing in E_{gs} configurations.

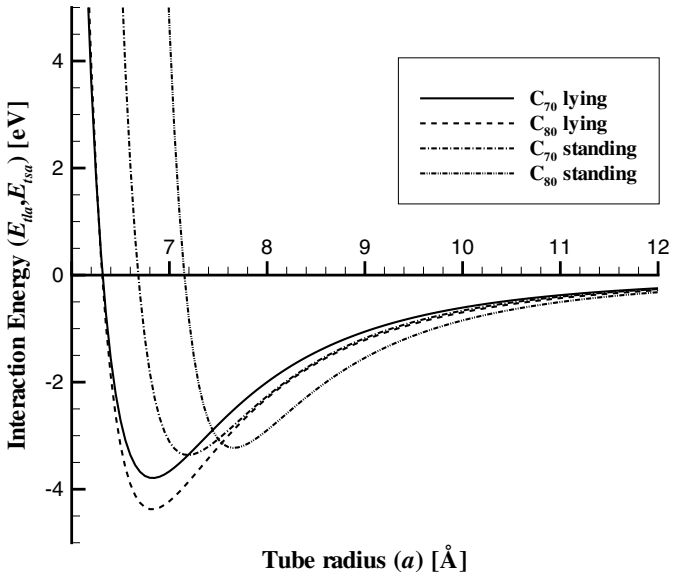

Figure 2. Interaction energy between carbon nanotube and axially centered fullerene, both lying in E_{tla} and standing in E_{tsa} configurations.

As we show in the following section, centrally located fullerenes are applicable for a large range of nanotube radii because the nanotube axis is the equilibrium location for the fullerene.

In figure 2, we show the interaction energies for axially centered spheroids in either the lying E_{tla} or the standing E_{tsa} orientations, using the expressions derived in appendices E and

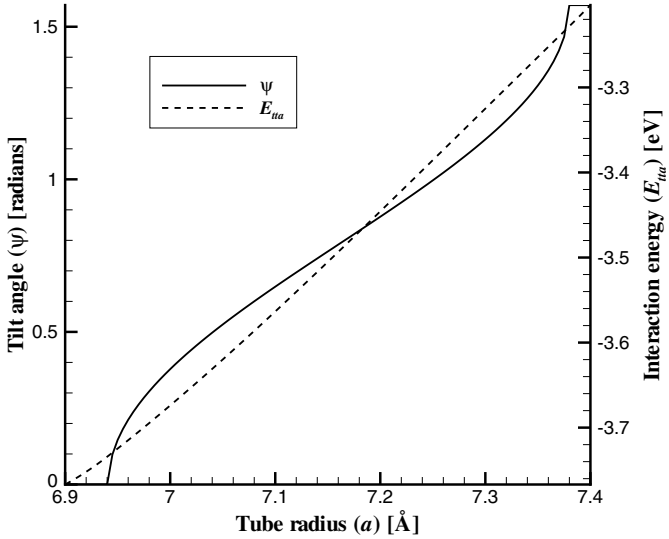

Figure 3. Interaction energy between carbon nanotube and an axially centered fullerene C_{70} tilting at an angle ψ to the nanotube axis.

F, respectively. As expected, the lying orientation is favored for smaller radius nanotubes, with the lying orientation resulting in an interaction energy of -3.792 eV for a C_{70} fullerene in a nanotube of radius 6.83 Å, and an interaction energy of -4.376 eV for a C_{80} fullerene encapsulated in a nanotube with a radius of 6.82 Å. For the standing orientation, the interaction energy reaches an extremum of -3.361 eV for a C_{70} fullerene inside a tube of radius 7.19 Å, and an extremum of -3.228 eV for a C_{80} fullerene within a nanotube of radius 7.66 Å.

From figure 2 it is clear that the lying configuration is favored for tubes below some threshold and the standing configuration is favored for tubes with a radius higher than this threshold. However, it is not expected that as the tube radius increases that the orientation would switch between these two possibilities. The expected behavior is that the spheroid would begin to tilt at some stage, and then make a smooth transition between the two extreme orientations. To examine this behavior we determine the minimum energy level for an axially centered fullerene with arbitrary tilt angle ψ. In figures 3 and 4, we note that the tilt angle ψ which leads to the least energy configuration for an axially centered spheroid varies smoothly from 0 to $\pi/2$ radians. For the C_{70} fullerene (as shown in figure 3), the fullerene begins tilting for a nanotube of radius 6.94 Å and then follows an approximately inverse-sine curve until a radius of 7.38 Å is reached when the spheroid is in the standing orientation. For the C_{80} fullerene (shown in figure 4) the same inverse-sine-like curve is shown between the nanotube radii values of 6.94 Å and 7.85 Å. This larger domain is expected and is due to the longer polar axis for this molecule.

3.3. Interaction of an axially offset spheroidal fullerene with a carbon nanotube

In this section, we investigate the various orientations of a single spheroidal fullerene inside an infinite carbon nanotube when the center of the spheroid lies off the axis of the nanotube. The offset issue becomes particularly important as the radius of the nanotube increases. This is because the equilibrium position for the fullerene is no longer on the axis of the nanotube,

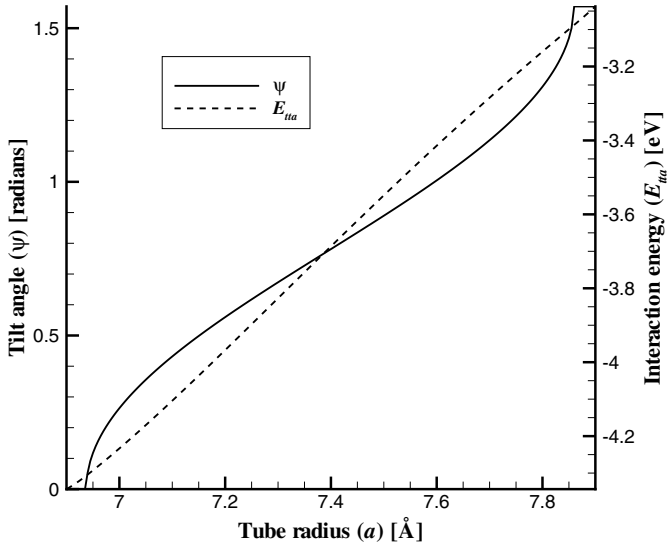

Figure 4. Interaction energy between carbon nanotube and an axially centered fullerene C_{80} tilting at an angle ψ to the nanotube axis.

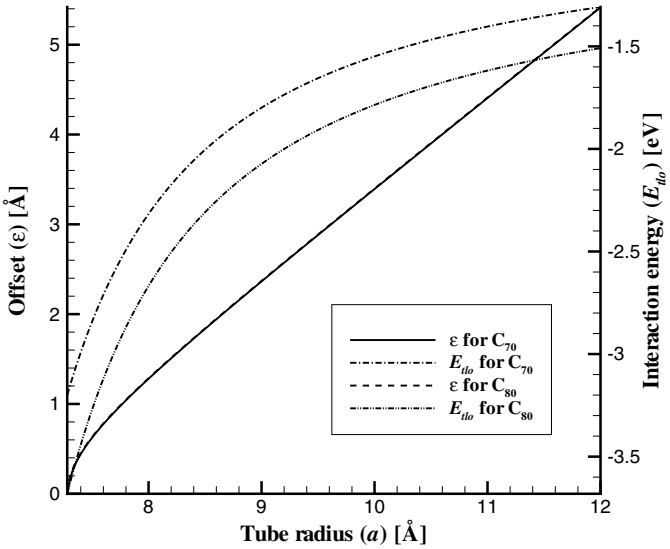

Figure 5. Offset distance ε and interaction energy E_{tlo} for a carbon nanotube and an offset fullerene C_{70} and C_{80} in a lying orientation.

and in order to assume a minimum energy configuration, the spheroid must move off-axis and adopt a location which is closer to the nanotube wall.

In figure 5, we show the offset ε and the resulting interaction energy E_{tlo} for spheroidal fullerenes C_{70} and C_{80} in a lying orientation, which are computed from the expressions derived in appendix H. The equilibrium offset position ε for the two fullerenes are almost indistinguishable, with the fullerene beginning to move off the nanotube axis when the tube

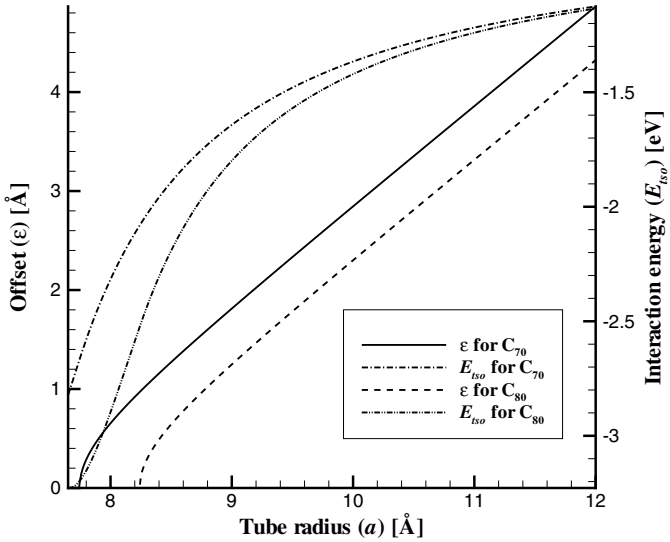

Figure 6. Offset distance ε and interaction energy E_{tlo} for a carbon nanotube and an offset fullerene C_{70} and C_{80} in a standing orientation.

radius exceeds 7.28 Å and initially it moves off the axis quite abruptly and quickly adopts a linear relationship with $\varepsilon \approx a - 6.55$, remembering that 6.55 Å is the equilibrium distance we calculate for a lying fullerene and flat graphene.

Figure 6 shows the equilibrium offset ε and resulting interaction energy E_{tso} for spheroidal fullerenes C_{70} and C_{80} in a standing orientation calculated from the expressions given in appendix I. In this case, the offset positions for the two different types of fullerenes are clearly distinct owing to the variation in polar axis length between the two molecules. The C_{70} fullerene begins to move off-axis once the nanotube radius exceeds 7.75 Å, and again it shows an abrupt movement off-axis which quickly settles down to an approximately linear relationship with the nanotube radius. That is $\varepsilon \approx a - 7.11$, and we comment that 7.11 Å is the equilibrium distance calculated earlier for graphene and a C_{70} fullerene in a standing orientation. Similarly, the C_{80} fullerene abruptly moves to an off-axis position once the radius exceeds 8.25 Å, and also quickly settles down to the linear relationship with nanotube radius $\varepsilon \approx a - 7.66$, which is again consistent with the equilibrium distance for flat graphene.

We now consider the equilibrium position of spheroidal fullerenes when the molecule is simultaneously allowed to move off-axis and also tilt in the direction of the displacement. As shown in figures 5 and 6 the lowest energy configuration for a C_{70} fullerene begins as standing on-axis and then moves to standing off-axis. As the nanotube radius approaches approximately 8 Å the lying off-axis begins to provide a lower interaction energy, so that perhaps there is a tilting off-axis configuration in this transition range which the molecule prefers to adopt. Using the expression for tilting offset fullerenes derived in appendix J, we examine the interaction energy E_{tto} for various offset distances ε and tilt angles ψ which are shown in figure 7. This plot shows that the lying and standing orientations both provide independent stable equilibrium orientations for this configuration. The depth of the well in both cases is approximately -2.32 eV and the offset positions are 0.65 Å for the lying orientation and 1.28 Å for the standing orientation. As a measure of the stability of these equilibrium positions we examine the depth of the highest point connecting these two wells.

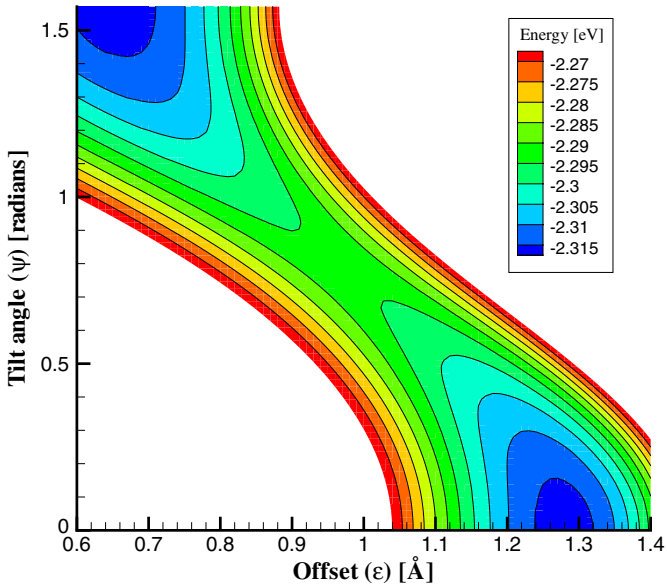

Figure 7. Contour plot of interaction energy E_{tto} for a C_{70} fullerene for a 8 Å radius nanotube, showing two distinct and approximately equal local minima.

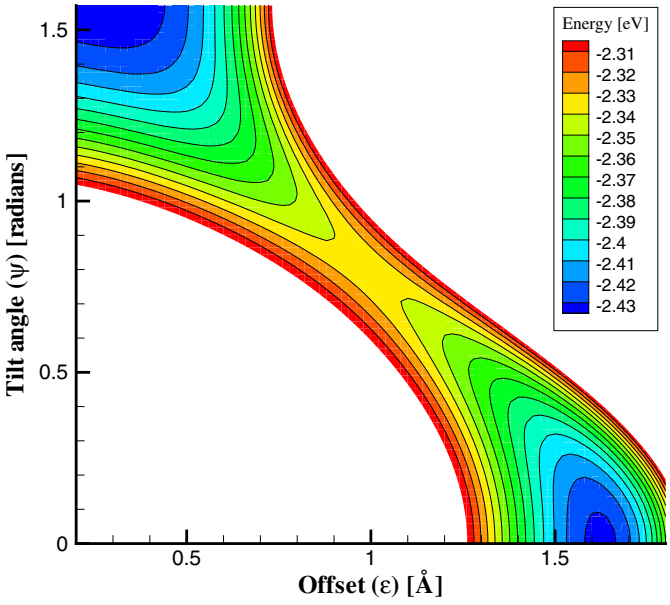

Figure 8. Contour plot of interaction energy E_{tto} for a C_{80} fullerene for a 8.3 Å radius nanotube, showing two distinct and approximately equal local minima.

It can be seen from the plot that this occurs at a depth of -2.29 eV and therefore the effective depth separating the two minima is approximately 0.03 eV.

In figure 8, we plot the interaction energy E_{tto} for a C_{80} fullerene and a carbon nanotube of radius 8.3 Å. This plot also shows two approximately equal equilibrium positions each with a

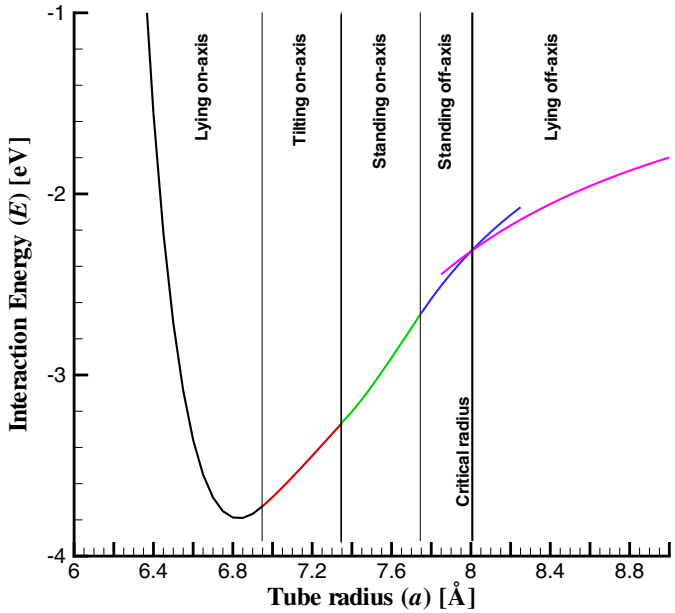

Figure 9. Overview plot of the various orientations for a C_{70} fullerene with five primary regimes identified. Note that in the vicinity of the critical radius of 8 Å two orientations are possible.

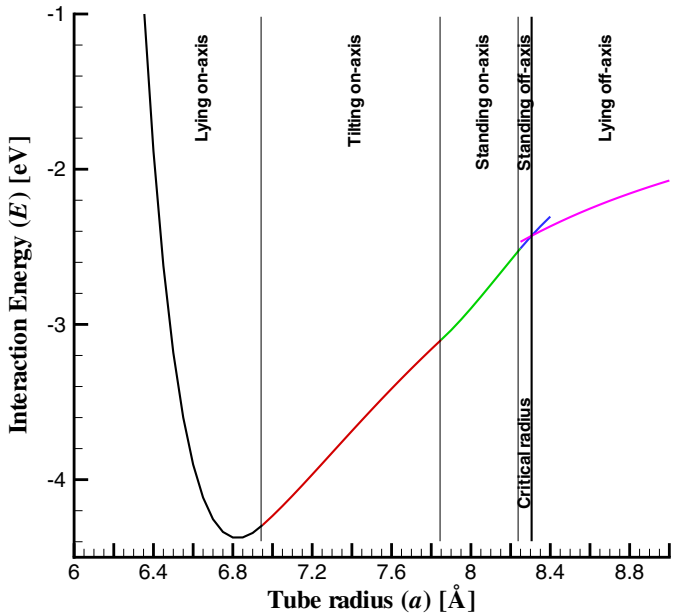

Figure 10. Overview plot of the various orientations for a C_{80} fullerene with five primary regimes identified. Note that in the vicinity of the critical radius of 8.3 Å two orientations are possible.

well depth of approximately −2.43 eV for the lying orientation and −2.44 eV for the standing orientation. These occur at an offset ε of 0.29 Å in the case of the standing orientation and

Table 2. Ranges of nanotube radii for C_{70} and C_{80} fullerenes in all identified regimes.

Regime	Configuration	C_{70} fullerene Tube radius (a) [Å]	C_{80} fullerene Tube radius (a) [Å]
1	Lying on-axis	6.32–6.94	6.32–6.94
2	Tilting on-axis	6.94–7.38	6.94–7.85
3	Standing on-axis	7.38–7.75	7.85–8.25
4	Standing off-axis	7.75–8.00	8.25–8.30
5	Lying off-axis	8.00–∞	8.30–∞

1.62 Å for the lying orientation. We again examine the least energy path connecting these two configurations and find that in this case this occurs at a depth of approximately -2.34 eV. This leads to an effective well depth of approximately 0.09 eV, which is three times deeper than in the C_{70} case and it can be attributed to the increased eccentricity of this molecule.

4. Conclusions

In this paper using analytical expressions derived in the appendices, we examine various orientations of spheroidal fullerenes interacting with graphene sheets and carbon nanotubes. When the fullerenes are fully encapsulated in carbon nanotubes we find that the equilibrium orientation depends primarily on the radius of the nanotube in question and five main regimes are identified. For small radii nanotubes, the fullerene adopts a lying orientation, which we designate as the first regime. As the radius increases the fullerene enters a second regime such that it begins to tilt until it has adopted a standing orientation which is still centered on the nanotube axis, and which we identify as the third regime. Following this transition, as the radius continues to increase, the fullerene adopts an off-axis location while maintaining a standing orientation, which we call the fourth regime. As the radius continues to increase a second equilibrium position becomes available to the molecule which is the lying and offset configuration, and for a critical range of nanotube radii these two configurations co-exist and are of comparable well-depth. However, as the radius continues to increase the depth of the standing orientation weakens as compared to that of the lying configuration, and the lying configuration dominates, as in the case of flat graphene, and this is referred to as the fifth and final regime.

As summarized in figure 9 for the C_{70} fullerene, the lying on-axis configuration is favored for radii less than 6.94 Å, a tilting orientation is adopted for radii in the range 6.94–7.38 Å. A standing on-axis configuration dominates for the nanotube radii in the range 7.38–7.75 Å. For radii greater than 7.75 Å the C_{70} molecule adopts an off-axis configuration. The orientation of the fullerene relative to the nanotube axis in this region again depends on radius. For nanotube radii of less than 8 Å the standing orientation is favored, but as the critical radius of 8 Å is reached a second equilibrium orientation is available to the molecule with an effective well-depth of 0.03 eV separating these two configurations. For nanotubes of radii in excess of 8 Å the standing orientation becomes less favored and the lying configuration dominates. This branching between distinct minima solutions accounts for the discontinuity in gradient at the critical radius value.

In figure 10, we also present a similar picture for the C_{80} molecule with a lying configuration for nanotubes of radii less than 6.94 Å, a tilting orientation in the range 6.94–7.85 Å and a standing orientation in the range 7.85–8.25 Å. For nanotubes of radii greater than 8.25 Å an offset configuration is favored, and the orientation which is preferred is standing

for radii less than 8.3 Å and the lying orientation for radii in excess of this value. For radii in the vicinity of this critical value of 8.3 Å two minimum configurations exist, both lying and standing separated by an effective well-depth of approximately 0.09 eV. As before, the branching between distinct minima solutions at the critical nanotube radius is the reason for the discontinuity in the gradient at this point.

The general results of this paper are summarized in table 2 and show good agreement with the results of Verberck and Michel [14] in terms of when the initiation of the intermediate tilting orientation. However, we find that this regime persists to a radius of 7.38 Å, whereas Verberck and Michel [14] find that a standing orientation is adopted once a radius of 7.2 Å is reached. The results for the lying and standing offset orientations presented in figures 5 and 6 agree very well with the same configurations in Verberck and Michel [14]. The results for C_{70} also agree well with the findings of Okada *et al* [6], who report that C_{70} molecules lie in a (17,0) nanotube with radius of approximately 6.6 Å, but stand in a (19,0) nanotube with a radius of approximately 7.4 Å. Likewise, Khlobystov *et al* [12] find that C_{70} molecules lie in a (10,10) nanotube with a radius of 6.78 Å and stand within an (11,11) nanotube with a radius of 7.46 Å, which again agrees well with the results presented here.

The significance of the present work is the derivation of the analytical expressions contained in the appendices which provide explicit formulae to calculate the energy of spheroidal fullerenes and nanotubes. Also of importance is the treatment of the tilting and offset configurations detailed in appendix J which evaluates integrals for a more general problem than has appeared previously, and does so without requiring any approximations or numerical integration methods. However, perhaps the most interesting result of this work is the finding that there exits two equally dominate local minima for certain critical radii, that is 8 Å for C_{70} molecules and 8.3 Å for C_{80} molecules. These configurations provide a situation such that the fullerene may adopt a lying or standing orientation with some known energy barrier standing between each state. This may provide configurations which may be exploited for a nano-computing memory device.

Acknowledgments

The authors are grateful to the Australian Research Council for their support through the Discovery Project Scheme and the provision of an Australian Postdoctoral Fellowship for NT and an Australian Professorial Fellowship for JMH.

Appendix A. Interaction of a plane with an arbitrary point

In this appendix, we derive an expression for the interaction of an infinite plane graphene sheet with a single point. The resulting expression is the starting point for the following two appendices which calculate the interaction for spheroidal surfaces in either a lying or standing orientation. We begin by adopting a three-dimensional Cartesian coordinate system (x, y, z), in which the plane is taken to be the xy-plane and the interacting point is taken to lie on the z-axis at a position ρ units from the origin, i.e. $(0, 0, \rho)$. We employ the Lennard–Jones potential function and we define the total interaction potential $E_{gp}(\rho)$ between the plane and the point by

$$E_{gp}(\rho) = \eta_g \left(-AC_3 + BC_6\right), \qquad C_n = \int_{-\infty}^{\infty}\int_{-\infty}^{\infty} (x^2 + y^2 + \rho^2)^{-n}\, \mathrm{d}x\, \mathrm{d}y,$$

where η_g is the atomic number density of the carbon atoms making up the graphene sheet, and A and B are the attractive and repulsive constants of the Lennard–Jones function, respectively.

We comment that, as expected this integral is singular if and only if $\rho = 0$. By employing the substitution $y = \sqrt{x^2 + \rho^2}\tan\chi$, the integral C_n becomes

$$\begin{aligned} C_n &= \int_{-\pi/2}^{\pi/2} \cos^{2n-2}\chi \,\mathrm{d}\chi \int_{-\infty}^{\infty} (x^2+\rho^2)^{1/2-n}\,\mathrm{d}x \\ &= 2^{2-2n}\pi \binom{2n-2}{n-1} \int_{-\infty}^{\infty} (x^2+\rho^2)^{1/2-n}\,\mathrm{d}x. \end{aligned}$$

Now we employ the substitution $x = \rho\tan\varphi$ which gives

$$C_n = (2\rho)^{2-2n}\pi \binom{2n-2}{n-1} \int_{-\pi/2}^{\pi/2} \cos^{2n-3}\varphi \,\mathrm{d}\varphi = \frac{\pi}{n-1}\rho^{2-2n},$$

which allows us to simply express the interaction between a point and a plane as given by

$$E_{gp}(\rho) = \pi\eta_g \left(-\frac{A}{2\rho^4} + \frac{B}{5\rho^{10}}\right). \tag{A.1}$$

We comment that (A.1) is used as the starting point for the following two appendices.

Appendix B. Interaction of a plane with a lying spheroid

In this appendix, we take equation (A.1) and use it to derive an expression for the total interaction energy E_{gl}, for a spheroidal fullerene and a graphene plane, when the polar axis of the spheroid is parallel to the plane but offset by some distance ε. This enables us to prescribe the location of an element on the surface of the spheroid with the following parametric equations

$$x = c\cos\phi_s, \qquad y = b\sin\theta_s\sin\phi_s, \qquad z = \varepsilon + b\cos\theta_s\sin\phi_s,$$

where b is the equatorial semi-axis length, c is the polar semi-axis length, $-\pi < \theta_s \leqslant \pi$, and $0 \leqslant \phi_s \leqslant \pi$. Since we take the graphene plane to be infinite in both directions we can ignore the x and y distances and simply integrate the z distance over the surface of the spheroid. Thus we can write the energy as

$$E_{gl} = \eta_s \int_0^{\pi}\int_{-\pi}^{\pi} E_{gp}(\varepsilon + b\cos\theta_s\sin\phi_s) b\sin\phi_s \sqrt{b^2\cos^2\phi_s + c^2\sin^2\phi_s}\,\mathrm{d}\theta_s\,\mathrm{d}\phi_s,$$

where η_s is the atomic surface density for the spheroid. By substituting (A.1) and rearrangement we can express this as

$$\begin{aligned} E_{gl} &= \pi\eta_g\eta_s bc\left(-\frac{A}{2}D_2 + \frac{B}{5}D_5\right), \\ D_n &= \int_{-\pi}^{\pi}\int_0^{\pi} (\varepsilon + b\sin\phi_s\cos\theta_s)^{-2n}\sin\phi_s(1-e^2\cos^2\phi_s)^{1/2}\,\mathrm{d}\phi_s\,\mathrm{d}\theta_s, \end{aligned} \tag{B.1}$$

where $e^2 = 1 - (b/c)^2$ is the usual squared elliptical eccentricity. First, we consider the θ_s integral noting that we can write this in the form

$$D^{\theta} = \int_{-\pi}^{\pi} (\varepsilon + b\sin\phi_s - 2b\sin\phi_s\sin^2(\theta_s/2))^{-2n}\,\mathrm{d}\theta_s.$$

Making the substitution $t = \sin^2(\theta_s/2)$ and by splitting the integration interval into two, and adding together yields

$$D^{\theta} = 2(\varepsilon + b\sin\phi_s)^{-2n}\int_0^1 t^{-1/2}(1-t)^{-1/2}\left(1 - \frac{2b\sin\phi_s}{\varepsilon + b\sin\phi_s}t\right)^{-2n}\mathrm{d}t.$$

We note that this is the fundamental integral form for the standard hypergeometric function $F(\alpha, \beta; \gamma; z)$, with $\alpha = 2n$, $\beta = 1/2$, $\gamma = 1$ and $z = 2b \sin\phi_s/(\varepsilon + b \sin\phi_s)$, which allows us to express D^θ exactly as

$$D^\theta = 2\pi(\varepsilon + b\sin\phi_s)^{-2n} F(2n, 1/2; 1; 2b\sin\phi_s/(\varepsilon + b\sin\phi_s)).$$

Here we employ the identity that $F(\alpha, \beta; \gamma; z) = (1-z)^{-\beta} F(\gamma - \alpha, \beta; \gamma; z/(z-1))$, which gives

$$D^\theta = 2\pi(\varepsilon + b\sin\phi_s)^{1/2-2n}(\varepsilon - b\sin\phi_s)^{-1/2} \times F(1-2n, 1/2; 1; -2b\sin\phi_s/(\varepsilon - b\sin\phi_s)),$$

and since $1 - 2n$ is a negative integer, this can be written as a terminating series containing $2n$ terms as

$$D^\theta = 2\pi(\varepsilon + b\sin\phi_s)^{1/2-2n} \sum_{m=0}^{2n-1} \frac{(1-2n)_m (1/2)_m (-2b\sin\phi_s)^m}{(m!)^2(\varepsilon - b\sin\phi_s)^{1/2+m}},$$

and we note that $(x)_n$ is the usual Pochhammer symbol defined by $(x)_n = \Gamma(x+n)/\Gamma(x)$. We now use the identities that

$$(-1)^m(1-2n)_m = \frac{(2n-1)!}{(2n-1-m)!},$$

when $m \leqslant 2n-1$ and $(1/2)_m = (2m)!/(2^{2m}m!)$ which yields

$$D^\theta = 2\pi(\varepsilon + b\sin\phi_s)^{1/2-2n} \times \sum_{m=0}^{2n-1} \binom{2n-1}{m} \binom{2m}{m} \left(\frac{b}{2}\right)^m \sin^m\phi_s (\varepsilon - b\sin\phi_s)^{-1/2-m},$$

and therefore the total integral D_n is given by

$$D_n = 2\pi \sum_{m=0}^{2n-1} \binom{2n-1}{m} \binom{2m}{m} \left(\frac{b}{2}\right)^m D^\phi,$$

$$D^\phi = \int_0^\pi \sin^{m+1}\phi_s (\varepsilon^2 - b^2\sin^2\phi_s)^{1/2-2n} (\varepsilon - b\sin\phi_s)^{2n-m-1} (1 - e^2\cos^2\phi_s)^{1/2}\, \mathrm{d}\phi_s.$$

We now expand the $(\varepsilon - b\sin\phi_s)^{2n-m-1}$ term as a binomial expansion to give

$$D^\phi = (\varepsilon^2 - b^2)^{1/2-2n} \sum_{p=0}^{2n-m-1} (-1)^p \binom{2n-m-1}{p} \varepsilon^{2n-m-p-1} b^p D^{\phi\star}$$

$$D^{\phi\star} = \int_0^\pi \sin^{m+p+1}\phi_s (1 + \lambda\cos^2\phi_s)^{1/2-2n} (1 - e^2\cos^2\phi_s)^{1/2}\, \mathrm{d}\phi_s,$$

where $\lambda = b^2/(\varepsilon^2 - b^2)$. Bisecting the interval and substituting $u = \cos^2\phi_s$ produces

$$D^{\phi\star} = \int_0^1 u^{-1/2}(1-u)^{(m+p)/2}(1+\lambda u)^{1/2-2n}(1-e^2u)^{1/2}\, \mathrm{d}u,$$

which is now in fundamental integral form for an Appell's hypergeometric function of two variables $F_1(\alpha, \beta, \beta', \gamma; x; y)$ and in this case, $\alpha = 1/2$, $\beta = 2n - 1/2$, $\beta' = -1/2$, $\gamma = (m+p+3)/2$, $x = -\lambda$ and $y = e^2$. The co-efficient of the function is $C = \Gamma(\alpha)\Gamma(\gamma-\alpha)/\Gamma(\gamma)$ which when we make the substitution $q = (m+p+1)/2$ becomes

$$C = \frac{\Gamma(1/2)\Gamma(q+1/2)}{\Gamma(q+1)}.$$

Employing Legendre's duplication formula we can write C as

$$C = \frac{\Gamma(1/2)^2\Gamma(2q+1)}{2^{2q}\Gamma(q+1)^2} = \frac{\pi}{2^{2q}}\binom{2q}{q},$$

and therefore

$$D^{\phi\star} = \frac{\pi}{2^{m+p+1}}\binom{m+p+1}{(m+p+1)/2} \times F_1(1/2, 2n-1/2, -1/2, (m+p+3)/2; -\lambda, e^2),$$

which now enables us to write the full analytical expression for D_n as

$$\begin{aligned} D_n = \pi^2\varepsilon^{2n-1}(\varepsilon^2-b^2)^{1/2-2n}\sum_{m=0}^{2n-1}\binom{2n-1}{m}\binom{2m}{m}\left(\frac{b}{4\varepsilon}\right)^m \\ \times \sum_{p=0}^{2n-m-1}(-1)^p\binom{2n-m-1}{p}\binom{m+p+1}{(m+p+1)/2}\left(\frac{b}{2\varepsilon}\right)^p \\ \times F_1(1/2, 2n-1/2, -1/2, (m+p+3)/2; -b^2/(\varepsilon^2-b^2), e^2). \end{aligned} \tag{B.2}$$

Appendix C. Interaction of a plane with a standing spheroid

In this appendix, we employ equation (A.1) to derive an expression for the total interaction energy E_{gs}, for a spheroidal fullerene and a graphene plane, for which the polar axis of the spheroid is perpendicular to the plane and the center of the spheroid is offset by some distance ε. As before we use the parametric form of the spheroidal surface as

$$x = b\cos\theta_s\sin\phi_s, \qquad y = b\sin\theta_s\sin\phi_s, \qquad z = \varepsilon + c\cos\phi_s,$$

where b is the equatorial semi-axis length, c is the polar semi-axis length, $-\pi < \theta_s \leqslant \pi$, and $0 \leqslant \phi_s \leqslant \pi$. As in appendix B we can ignore the x and y distances and simply integrate the z distance over the surface of the spheroid, and thus the energy is given by

$$E_{gs} = \eta_s\int_0^{\pi}\int_{-\pi}^{\pi} E_{gp}(\varepsilon + c\cos\phi_s)b\sin\phi_s\sqrt{b^2\cos^2\phi_s + c^2\sin^2\phi_s}\,\mathrm{d}\theta_s\,\mathrm{d}\phi_s,$$

where η_s is the atomic surface density for the spheroid. By substituting (A.1) and rearrangement we can express this as

$$\begin{aligned} E_{gs} &= \pi\eta_g\eta_s bc\left(-\frac{A}{2}G_2 + \frac{B}{5}G_5\right), \\ G_n &= \int_{-\pi}^{\pi}\int_0^{\pi}(\varepsilon + c\cos\phi_s)^{-2n}\sin\phi_s(1-e^2\cos^2\phi_s)^{1/2}\,\mathrm{d}\phi_s\,\mathrm{d}\theta_s, \end{aligned} \tag{C.1}$$

where, as before, $e^2 = 1-(b/c)^2$ is the squared elliptical eccentricity. We note that the integrand in this case does not depend on θ_s enabling the integration to be performed immediately. The remaining integral can then be rearranged to yield

$$G_n = 2\pi\int_0^{\pi}(\varepsilon^2 - c^2\cos^2\phi_s)^{-2n}(\varepsilon - c\cos\phi_s)^{2n}\sin\phi_s(1-e^2\cos^2\phi_s)^{1/2}\,\mathrm{d}\phi_s,$$

so that by expanding $(\varepsilon - c\cos\phi_s)^{2n}$ as a binomial gives

$$G_n = 2\pi\varepsilon^{-2n}\sum_{m=0}^{2n}(-1)^m\binom{2n}{m}\left(\frac{c}{\varepsilon}\right)^m G^{\phi}, \tag{C.2}$$

$$G^{\phi} = \int_0^{\pi} \sin\phi_s \cos^m \phi_s \left[1 - \frac{c^2}{\varepsilon^2}\cos^2\phi_s\right]^{-2n} (1 - e^2\cos^2\phi_s)^{1/2}\,\mathrm{d}\phi_s. \quad \text{(C.3)}$$

The next observation is that by bisecting the interval of integration and making the substitution $\phi^{\star} = \pi - \phi_s$ we find that $G^{\phi} = 0$ when m is odd. Therefore we replace $m \to 2m$ in (C.2) and (C.3) which gives

$$G_n = 2\pi\varepsilon^{-2n} \sum_{m=0}^{n} \binom{2n}{2m} \left(\frac{c}{\varepsilon}\right)^{2m} G^{\phi},$$

$$G^{\phi} = \int_0^{\pi} \sin\phi_s \cos^{2m}\phi_s \left(1 - \frac{c^2}{\varepsilon^2}\cos^2\phi_s\right)^{-2n} (1 - e^2\cos^2\phi_s)^{1/2}\,\mathrm{d}\phi_s.$$

Bisecting the interval of integration and substituting $u = \cos^2\phi_s$ yields

$$G^{\phi} = \int_0^{1} u^{m-1/2} \left(1 - \frac{c^2}{\varepsilon^2}u\right)^{-2n} (1 - e^2 u)^{1/2}\,\mathrm{d}u,$$

which is the fundamental integral form for the Appell's hypergeometric function $F_1(\alpha, \beta, \beta', \gamma; x, y)$ with $\alpha = m+1/2$, $\beta = 2n$, $\beta' = -1/2$, $\gamma = m+3/2$, $x = c^2/\varepsilon^2$, $y = e^2$. In this case the, coefficient C is given by

$$C = \frac{\Gamma(m + 1/2)\Gamma(1)}{\Gamma(m + 3/2)} = \frac{2}{2m + 1},$$

which lets us give the total expression for G_n in the following way:

$$G_n = 4\pi\varepsilon^{-2n} \sum_{m=0}^{n} \frac{(2n)!}{(2m + 1)!(2n - 2m)!} \left(\frac{c}{\varepsilon}\right)^{2m} \times F_1(m + 1/2, 2n, -1/2, m + 3/2; (c/\varepsilon)^2, 1 - (b/c)^2). \quad \text{(C.4)}$$

Appendix D. Interaction of a carbon nanotube with an arbitrary point

We begin by deriving an expression for the interaction of an infinite carbon nanotube with an arbitrary point. The resulting expression becomes the starting point for all other interaction energies since it is integrated over the surface of the interacting fullerene. The surface of the carbon nanotube in Cartesian coordinates is given by the following parametric form:

$$x = a\cos\theta_t, \qquad y = a\sin\theta_t, \qquad z = z_t,$$

where a is the radius of the carbon nanotube, $-\pi < \theta_t \leqslant \pi$ and $-\infty < z_t < \infty$. As the tube is doubly infinite and radially symmetric we can assume, without loss of generality, that the point P of interaction is fully prescribed by a distance ρ from the z-axis and is given by the coordinates $P = (\rho, 0, 0)$. We define r to the distance from P to a typical point on the surface of the nanotube and therefore we may write

$$r = [(a\cos\theta_t - \rho)^2 + a^2\sin^2\theta_t + z_t^2]^{1/2},$$

and by employing the Lennard–Jones potential function we have that the interaction potential $E_{tp}(\rho)$ between the tube and any point is given by

$$E_{tp}(\rho) = \eta_t(-AH_3 + BH_6), \qquad H_n = a\int_{-\pi}^{\pi}\int_{-\infty}^{\infty} r^{-2n}\,\mathrm{d}z_t\,\mathrm{d}\theta_t,$$

where η_t is the atomic surface density for the carbon nanotube, and A and B are the Lennard–Jones constants of attraction and repulsion, respectively.

We begin by defining $\lambda^2 = (a\cos\theta_t - \rho)^2 + a^2\sin^2\theta_t$, and then by making the substitution $z_t = \lambda\tan\chi$, we obtain the integral

$$H_n = a\int_{-\pi/2}^{\pi/2}\cos^{2(n-1)}\chi\,\mathrm{d}\chi\int_{-\pi}^{\pi}\lambda^{1-2n}\,\mathrm{d}\theta_t,$$

and the χ integral can be performed immediately using Gradshteyn and Ryzhik [23, equation 3.621(3)], which we rearrange to yield

$$H_n = \frac{\pi a(2n-2)!}{2^{2n-2}[(n-1)!]^2}\int_{-\pi}^{\pi}\lambda^{1-2n}\,\mathrm{d}\theta_t.$$

We now consider the θ_t integral which we denote by $H_{\theta,n}$ and we rearrange λ to give

$$H_{\theta,n} = \int_{-\pi}^{\pi}[(a-\rho)^2 + 4a\rho\sin^2(\theta_t/2)]^{1/2-n}\,\mathrm{d}\theta_t.$$

By splitting the interval and making the substitution $t = \sin^2(\theta_t/2)$ we may write

$$H_{\theta,n} = 2(a-\rho)^{1-2n}\int_0^1 t^{-1/2}(1-t)^{-1/2}\{1+[4a\rho/(a-\rho)^2]t\}^{1/2-n}\,\mathrm{d}t,$$

and this is the fundamental integral form for the standard hypergeometric function $F(\alpha,\beta;\gamma;z)$, which yields

$$H_{\theta,n} = 2\pi(a-\rho)^{1-2n}F(n-1/2,1/2;1;-4a\rho/(a-\rho)^2),$$

and we note that in this case the hypergeometric function has the form $F(\alpha,\beta;2\beta;z)$ and therefore admits a quadratic transformation [24, section 2.11, equation (31)] which gives

$$H_{\theta,n} = 2\pi a^{1-2n}F(n-1/2,n-1/2;1;\rho^2/a^2),$$

which we also note can be expanded as the series

$$H_{\theta,n} = 2\pi a^{1-2n}\sum_{m=0}^{\infty}\left(\frac{\rho^m(n-1/2)_m}{a^m m!}\right)^2,$$

where again $(x)_n = \Gamma(x+n)/\Gamma(x)$ is the Pochhammer symbol. From the Legendre duplication formula we may show that

$$\Gamma(n-1/2) = \frac{\pi^{1/2}\Gamma(2n-1)}{2^{2n-2}\Gamma(n)},$$

and therefore

$$\begin{aligned}(n-1/2)_m &= \frac{\Gamma(n+m-1/2)}{\Gamma(n-1/2)} = \frac{\Gamma(2n+2m-1)\Gamma(n)}{2^{2m}\Gamma(n+m)\Gamma(2n-1)}\\ &= \frac{(n-1)!}{(2n-2)!}\cdot\frac{(2n+2m-2)!}{2^{2m}(n+m-1)!}.\end{aligned}$$

Substituting this term allows further simplification such that the total term H_n can be expressed simply as

$$H_n = \frac{8\pi^2a^2}{(2a)^{2n}(2n-2)!}\sum_{m=0}^{\infty}\left(\frac{\rho^m(2n+2m-2)!}{(4a)^m m!(n+m-1)!}\right)^2. \tag{D.1}$$

We comment that (D.1) is the starting point of all subsequent integral evaluations analyzed in these appendices. Since we take the tube radius a to be fixed, the only terms requiring further integration are those involving ρ which means that we are required to integrate functions of the form ρ^{2m}, where m is a non-negative integer.

Appendix E. Interaction with a lying and axially centered spheroid

In this appendix, we take equation (D.1) and use it to derive an expression for the interaction energy for a spheroidal fullerene inside an infinitely long carbon nanotube with the polar axis of the spheroid collinear with the nanotube axis. This means that we can prescribe the location of an element on the surface of the spheroid with the following parametric equations

$$x = b\cos\theta_s \sin\phi_s, \qquad y = b\sin\theta_s \sin\phi_s, \qquad z = c\cos\phi_s,$$

where b is the equatorial semi-axis length, c is the polar semi-axis length, $-\pi < \theta_s \leqslant \pi$, and $0 \leqslant \phi_s \leqslant \pi$. Since we are considering an infinite nanotube the z-coordinate is of no consequence and we need only consider the perpendicular displacement from the z-axis, and in this case $\rho = b\sin\phi_s$. Therefore, using the expression for $E_{tp}(\rho)$ from appendix D we can state the interaction energy E_{tla} for a lying spheroid to be given by

$$E_{tla} = \eta_s \int_0^{\pi}\int_{-\pi}^{\pi} E_{tp}(\rho) b \sin\phi_s (b^2\cos^2\phi_s + c^2\sin^2\phi_s)^{1/2}\,\mathrm{d}\theta_s\,\mathrm{d}\phi_s,$$

where η_s is the atomic surface density for the spheroidal fullerene. We note that the integrand does not depend on θ_s and therefore we can immediately evaluate this to give

$$E_{tla} = 2\pi bc\eta_s \int_0^{\pi} E_{tp}(\rho)\sin\phi_s\{1 - [(c^2 - b^2)/c^2]\cos^2\phi_s\}^{1/2}\,\mathrm{d}\phi_s.$$

Substituting for $E_{tp}(\rho)$ and expanding gives

$$E_{tla} = 16\pi^3 a^2 bc\eta_t\eta_s(-AI_3 + BI_6),$$

$$I_n = \frac{1}{(2a)^{2n}(2n-2)!}\sum_{m=0}^{\infty}\left(\frac{b^m(2n+2m-2)!}{(4a)^m m!(n+m-1)!}\right)^2 I_{\phi,m},$$

$$I_{\phi,m} = \int_0^{\pi}(\sin^2\phi_s)^{m+1/2}\{1 - [(c^2 - b^2)/c^2]\cos^2\phi_s\}^{1/2}\,\mathrm{d}\phi_s.$$

Now by using the substitution $t = \cos^2\phi_s$ we deduce

$$I_{\phi,m} = \int_0^1 t^{-1/2}(1-t)^m\{1 - [1 - (b/c)^2]t\}^{1/2}\,\mathrm{d}t,$$

which is in fundamental integral form for the usual hypergeometric function and therefore

$$I_{\phi,m} = \frac{2^{2m+1}(m!)^2}{(2m+1)!}F(-1/2, 1/2; m + 3/2; 1 - (b/c)^2),$$

where we have again used the Legendre duplication formula to express the coefficient in terms of simple factorial terms. In this paper, we evaluate the hypergeometric functions using the numerical package MAPLE. However, we comment that the argument of the hypergeometric function is the eccentricity squared $e^2 = 1 - (b/c)^2$, and for cases when the eccentricity is low (such as the with the C_{70} and C_{80} fullerenes of interest here), then the series expansion of this function converges quickly. In the special case of eccentricity $e = 0$, then the hypergeometric function takes the value of unity.

Appendix F. Interaction with a standing and axially centered spheroid

In this appendix, we proceed as in appendix E, except that instead of the spheroidal polar axis lying on the z-axis, it lies perpendicular to it. In this case, the parametric equations for the surface of the spheroid are given by

$$x = b\cos\theta_s \sin\phi_s, \qquad y = c\cos\phi_s, \qquad z = b\sin\theta_s \sin\phi_s,$$

where, as before, $-\pi < \theta_s \leqslant \pi$ and $0 \leqslant \phi_s \leqslant \pi$. In this case $\rho^2 = b^2 \cos^2\theta_s \sin^2\phi_s + c^2 \cos^2\phi_s$, which leads to slightly more complicated expressions to integrate. Using the expression for the interaction of a nanotube and a point $E_{tp}(\rho)$ derived in appendix D the interaction energy for a nanotube and a standing spheroid is given by

$$E_{tsa} = \eta_s \int_0^{\pi} \int_{-\pi}^{\pi} E_{tp}(\rho) b \sin\phi_s (b^2 \cos^2\phi_s + c^2 \sin^2\phi_s)^{1/2} \, \mathrm{d}\theta_s \, \mathrm{d}\phi_s,$$

but in this case the θ_s integration is by no means trivial. We define this integration by

$$J_{\theta,m} = \int_{-\pi}^{\pi} (b^2 \cos^2\theta_s \sin^2\phi_s + c^2 \cos^2\phi_s)^m \, \mathrm{d}\theta_s,$$

which we rearrange to become

$$J_{\theta,m} = c^{2m} \cos^{2m}\phi_s \int_{-\pi}^{\pi} (1 + (b/c)^2 \tan^2\phi_s \cos^2\theta_s)^m \, \mathrm{d}\theta_s,$$

and substituting $t = \cos^2\theta_s$ yields

$$J_{\theta,m} = 2c^{2m} \cos^{2m}\phi_s \int_0^1 t^{-1/2}(1-t)^{-1/2}(1 + (b/c)^2 \tan^2\phi_s t)^m \, \mathrm{d}t,$$

which again is in the fundamental integral form for the usual hypergeometric function. We can therefore write this as

$$J_{\theta,m} = 2\pi c^{2m} \cos^{2m}\phi_s F\left(-m, 1/2; 1; -\frac{b^2 \sin^2\phi_s}{c^2 \cos^2\phi_s}\right).$$

We note that $-m$ is a negative integer and therefore the hypergeometric function can be expanded as a terminating series, which can be written as

$$J_{\theta,m} = 2\pi c^{2m} \cos^{2m}\phi_s \sum_{k=0}^{m} \frac{(-m)_k (1/2)_k}{(k!)^2} (-1)^k \left(\frac{b \sin\phi_s}{c \cos\phi_s}\right)^{2k}.$$

Now by substituting $(1/2)_k = (2k)!/(2^{2k}k!)$ and when $k \leqslant m$ then $(-1)^k(-m)_k = m!/(m-k)!$, we derive

$$J_{\theta,m} = 2\pi c^{2m} \cos^{2m}\phi_s \sum_{k=0}^{m} \frac{m!(2k)!}{2^{2k}(m-k)!(k!)^3} \left(\frac{b \sin\phi_s}{c \cos\phi_s}\right)^{2k},$$

and we note that the factorial terms can be also expressed as a product of two binomial terms, thus

$$J_{\theta,m} = 2\pi c^{2m} \cos^{2m}\phi_s \sum_{k=0}^{m} \binom{m}{k} \binom{2k}{k} \left(\frac{b \sin\phi_s}{2c \cos\phi_s}\right)^{2k},$$

which is the form we use for the remainder of this appendix. We may now write the total interaction energy as

$$E_{tsa} = 16\pi^3 a^2 bc \eta_t \eta_s (-A J_3 + B J_6),$$

$$J_n = \frac{1}{(2a)^{2n}(2n-2)!} \sum_{m=0}^{\infty} \left(\frac{c^m (2n+2m-2)!}{(4a)^m m!(n+m-1)!}\right)^2 \sum_{k=0}^{m} \binom{m}{k} \binom{2k}{k} \left(\frac{b}{2c}\right)^{2k} J_{\phi,m,k},$$

$$J_{\phi,m,k} = \int_0^{\pi} (\sin^2\phi_s)^{k+1/2} (\cos^2\phi_s)^{m-k} \{1 - [(c^2 - b^2)/c^2] \cos^2\phi_s\}^{1/2} \, \mathrm{d}\phi_s.$$

Here we employ the substitution $t = \cos^2\phi_s$ to derive

$$J_{\phi,m,k} = \int_0^1 t^{m-k-1/2} (1-t)^k \{1 - [1 - (b/c)^2]t\}^{1/2} \, \mathrm{d}t,$$

which we again note is an integral form of the usual hypergeometric function and therefore

$$J_{\phi,m,k} = \frac{2^{2k+1} m!k!(2m-2k)!}{(m-k)!(2m+1)!} F(-1/2, m-k+1/2; m+3/2; 1-(b/c)^2).$$

We note that the some of the factorial terms in this equation simplify which allows J_n to be written more simply as

$$\begin{aligned} J_n = \frac{2}{(2a)^{2n}(2n-2)!} \sum_{m=0}^{\infty} \left(\frac{c^m (2n+2m-2)!}{(4a)^m (n+m-1)!} \right)^2 \frac{1}{(2m+1)!} \\ \times \sum_{k=0}^{m} \binom{2m-2k}{m-k} \binom{2k}{k} \left(\frac{b}{c}\right)^{2k} \\ \times F(-1/2, m-k+1/2; m+3/2; 1-(b/c)^2). \end{aligned}$$

This expression can now be evaluated with a numerical package or via a series expansion since again we note that the argument is the square of the eccentricity e, and in those fullerenes examined here, e is very close to zero.

Appendix G. Interaction with a tilting and axially centered spheroid

Here we derive the solution for the interaction energy E_{tta} for a spheroid which is centered on the origin and which is rotated about the x-axis by some arbitrary angle ψ. The rotation produces the following parametric form of the spheroidal surface:

$$\begin{aligned} x &= b\cos\theta_s \sin\phi_s, \qquad y = b\sin\theta_s \sin\phi_s \cos\psi - c\cos\phi_s \sin\psi, \\ z &= c\cos\phi_s \cos\psi + b\sin\theta_s \sin\phi_s \sin\psi, \end{aligned}$$

where $-\pi < \theta_s \leqslant \pi$ and $0 \leqslant \phi_s \leqslant \pi$, and therefore

$$\begin{aligned} \rho^2 &= b^2 \cos^2\theta_s \sin^2\phi_s + (b\sin\theta_s \sin\phi_s \cos\psi - c\cos\phi_s \sin\psi)^2 \\ &= \mu - \nu \sin\theta_s - \xi \sin^2\theta_s, \end{aligned}$$

where μ, ν and ξ are defined by

$$\begin{aligned} \mu &= b^2 + (c^2 \sin^2\psi - b^2)\cos^2\phi_s, \qquad \nu = 2bc \sin\psi \cos\psi \sin\phi_s \cos\phi_s, \\ \xi &= b^2 \sin^2\psi \sin^2\phi_s. \end{aligned}$$

Expanding ρ^{2m} using the multinomial theorem gives

$$\rho^{2m} = \sum_{p=0}^{m} \sum_{q=0}^{m-p} (-1)^{p+q} \frac{m!}{p!q!(m-p-q)!} \mu^{m-p-q} \nu^p \xi^q \sin^{p+2q}\theta_s.$$

Therefore we define the θ_s integration as we have done in the previous appendices

$$K_{\theta,m} = \sum_{p=0}^{m} \sum_{q=0}^{m-p} (-1)^{p+q} \frac{m!}{p!q!(m-p-q)!} \mu^{m-p-q} \nu^p \xi^q \int_{-\pi}^{\pi} \sin^{p+2q}\theta_s \, \mathrm{d}\theta_s,$$

and we note that the integral is zero whenever p is odd and so we replace the $p \to 2p$ giving

$$K_{\theta,m} = \sum_{p=0}^{\lfloor m/2 \rfloor} \sum_{q=0}^{m-2p} (-1)^q \frac{m!}{(2p)!q!(m-2p-q)!} \mu^{m-2p-q} \nu^{2p} \xi^q \int_{-\pi}^{\pi} \sin^{2(p+q)}\theta_s \, \mathrm{d}\theta_s,$$

where $\lfloor x \rfloor$ signifies the largest integer not greater than x and we note that

$$\int_{-\pi}^{\pi} \sin^{2(p+q)}\theta_s \, \mathrm{d}\theta_s = \frac{2\pi}{2^{2p+2q}} \binom{2(p+q)}{p+q}.$$

On expanding μ^{m-2p-q} using the binomial theorem we obtain

$$\mu^{m-2p-q} = \sum_{r=0}^{m-2p-q} \binom{m-2p-q}{r} b^{2m-4p-2q-2r} (c^2 \sin^2\psi - b^2)^r \cos^{2r}\phi_s.$$

This allows us to write the interaction energy E_{tta} for a tilting spheroid as

$$E_{tta} = 16\pi^3 a^2 bc\eta_t\eta_s(-AK_3 + BK_6),$$

$$K_n = \frac{1}{(2a)^{2n}(2n-2)!} \sum_{m=0}^{\infty} \left[\frac{b^m (2n+2m-2)!}{(4a)^m m!(n+m-1)!} \right]^2 \times \sum_{p=0}^{\lfloor m/2 \rfloor} \sum_{q=0}^{m-2p} (-1)^q \binom{2(p+q)}{p+q} \frac{m! c^{2p} \sin^{2p+2q}\psi \cos^{2p}\psi}{(2p)!q!(m-2p-q)!2^{2q} b^{2p}} \times \sum_{r=0}^{m-2p-q} \binom{m-2p-q}{r} \left(\frac{c^2 \sin^2\psi - b^2}{b^2} \right)^r K_\phi,$$

$$K_\phi = \int_0^\pi \cos^{2p+2r}\phi_s \sin^{2p+2q+1}\phi_s (1 - e^2\cos^2\phi_s)^{1/2} \, \mathrm{d}\phi_s.$$

Making the substitution $t = \cos^2\phi_s$ simplifies this last integral to

$$K_\phi = \int_0^1 t^{p+r-1/2}(1-t)^{p+q}(1-e^2 t)^{1/2} \, \mathrm{d}t.$$

We note that this K_ϕ is now in the integral form for the usual hypergeometric function $F(\alpha, \beta; \gamma; z)$, as described and can represented as

$$K_\phi = 2^{2p+2q+1} \frac{(2p+2r)!(2p+q+r)!(p+q)!}{(4p+2q+2r+1)!(p+r)!} \times F(-1/2, p+r+1/2; 2p+q+r+3/2; 1-(b/c)^2),$$

where we have used the Legendre duplication formula to express the coefficients in terms of simple factorials.

Appendix H. Interaction with a lying and offset spheroid

In this appendix, we derive a solution for the case of the spheroid lying with its polar axis parallel to the z-axis but offset from that axis by some distance, ε. Without loss of generality we can assume that this displacement is in the positive x-direction and therefore the parametric form of the spheroidal surface is given by

$$x = \varepsilon + b\cos\theta_s \sin\phi_s, \qquad y = b\sin\theta_s \sin\phi_s, \qquad z = c\cos\phi_s,$$

where $-\pi < \theta_s \leqslant \pi$ and $0 \leqslant \phi_s \leqslant \pi$, and therefore

$$\rho^2 = (\varepsilon + b\cos\theta_s \sin\phi_s)^2 + b^2 \sin^2\theta_s \sin^2\phi_s = (\varepsilon + b\sin\phi_s)^2 - 4\varepsilon b \sin\phi_s \sin^2(\theta_s/2).$$

We now use the expression derived in appendix D to express the interaction energy E_{tlo} for the configuration of an infinite nanotube and an offset spheroidal fullerene with

$$E_{tlo} = \eta_s \int_0^\pi \int_{-\pi}^\pi E_{tp}(\rho) b \sin\phi_s (b^2\cos^2\phi_s + c^2\sin^2\phi_s)^{1/2} \, \mathrm{d}\theta_s \, \mathrm{d}\phi_s,$$

but as in appendix F the θ_s integration is by no means trivial and so we define this integral by

$$L_{\theta,m} = \int_{-\pi}^{\pi} [(\varepsilon + b\sin\phi_s)^2 - 4\varepsilon b \sin\phi_s \sin^2(\theta_s/2)]^m \, \mathrm{d}\theta_s.$$

By using the substitution $t = \sin^2(\theta_s/2)$ we can transform this integral into

$$L_{\theta,m} = 2(\varepsilon + b\sin\phi_s)^{2m} \int_0^1 t^{-1/2}(1-t)^{-1/2} \left(1 - \frac{4\varepsilon b \sin\phi_s}{(\varepsilon + b\sin\phi_s)^2} t\right)^m \mathrm{d}t,$$

which is the integral form of the usual hypergeometric function, which allows us to express it as

$$L_{\theta,m} = 2\pi(\varepsilon + b\sin\phi_s)^{2m} F\left(-m, 1/2; 1; \frac{4\varepsilon b\sin\phi_s}{(\varepsilon + b\sin\phi_s)^2}\right).$$

Since the hypergeometric function is of the form $F(\alpha, \beta; 2\beta; z)$ it admits the quadratic transformation given in Erdélyi *et al* [24, section 2.11, equation (31)], which yields

$$L_{\theta,m} = 2\pi\varepsilon^{2m} F(-m, -m; 1; b^2 \sin^2\phi_s/\varepsilon^2).$$

We note that the series representation of this function terminates and therefore on expressing this as a series we obtain

$$L_{\theta,m} = 2\pi\varepsilon^{2m} \sum_{k=0}^{m} \left[\frac{(-m)_k}{k!}\left(\frac{b\sin\phi_s}{\varepsilon}\right)^k\right]^2.$$

We note that we can multiply the series term by $(-1)^{2k}$ and since $k \leqslant m$ we can replace $(-1)^k(-m)_k = m!/(m-k)!$ which can then be combined with the other factorial term to produce a binomial coefficient, which gives

$$L_{\theta,m} = 2\pi\varepsilon^{2m} \sum_{k=0}^{m} \left[\binom{m}{k}\left(\frac{b\sin\phi_s}{\varepsilon}\right)^k\right]^2.$$

Now taking the expression derived in appendix D we can give the interaction energy E_{tlo} of the offset spheroid as

$$E_{tlo} = 16\pi^3 a^2 bc\eta_t\eta_s\,(-AL_3 + BL_6),$$

$$L_n = \frac{1}{(2a)^{2n}(2n-2)!} \sum_{m=0}^{\infty} \left(\frac{\varepsilon^m(2n+2m-2)!}{(4a)^m m!(n+m-1)!}\right)^2 \sum_{k=0}^{m} \left[\binom{m}{k}\left(\frac{b}{\varepsilon}\right)^k\right]^2 L_{\phi,k},$$

$$L_{\phi,k} = \int_0^{\pi} (\sin^2\phi_s)^{k+1/2}\{1 - [(c^2-b^2)/c^2]\cos^2\phi_s\}^{1/2}\,\mathrm{d}\phi_s,$$

and we note $L_{\phi,k} = J_{\phi,k}$ as evaluated in appendix E and therefore

$$L_{\phi,k} = \frac{2^{2k+1}(k!)^2}{(2k+1)!} F(-1/2, 1/2; k+3/2; 1-(b/c)^2).$$

We comment that as before the series expansion of this hypergeometric function converges quickly for spheroids with small eccentricities. We also note that in the case of zero offset $\varepsilon = 0$, then all terms in the k series go to zero except for $k = m$, the end result being the E_{tlo} solution collapses to precisely the axially centered solution E_{tla} derived in appendix E.

Appendix I. Interaction with a standing and offset spheroid

In this appendix, we examine the case of the spheroid in a standing orientation with an additional offset from the z-axis by a distance ε. In this case, we cannot assume that the displacement is in a particular direction without loss of generality. However since the spheroids of interest (C_{70} and C_{80} fullerenes) are prolate, it is consistent to consider a displacement in the direction of the polar axis of the spheroid, which we set as the y-direction, and the parametric form of the spheroidal surface is given by

$$x = b\cos\theta_s \sin\phi_s, \qquad y = \varepsilon + c\cos\phi_s, \qquad z = b\cos\theta_s \sin\phi_s,$$

where $-\pi < \theta_s \leqslant \pi$ and $0 \leqslant \phi_s \leqslant \pi$, and therefore

$$\rho^2 = b^2\cos^2\theta_s \sin^2\phi_s + (\varepsilon + c\cos\phi_s)^2 = (\varepsilon + c\cos\phi_s)^2(1 + \lambda^2\cos^2\theta_s),$$

where $\lambda = b\sin\phi_s/(\varepsilon + c\cos\phi_s)$. So as before using the expression derived in appendix D we express the interaction energy E_{tso} for the configuration of a standing spheroid which is offset by

$$E_{tso} = \eta_s \int_0^{\pi}\int_{-\pi}^{\pi} E_{tp}(\rho) b\sin\phi_s (b^2\cos^2\phi_s + c^2\sin^2\phi_s)^{1/2}\,\mathrm{d}\theta_s\,\mathrm{d}\phi_s.$$

As before, neither of the integrations are trivial and we begin by defining the θ_s integration by

$$M_{\theta,m} = \int_{-\pi}^{\pi} (1 + \lambda^2\cos^2\theta_s)^m\,\mathrm{d}\theta_s.$$

By using the substitution $t = \cos^2\theta_s$ we transform this integral into the form

$$M_{\theta,m} = 2\int_0^1 t^{-1/2}(1-t)^{-1/2}(1+\lambda^2 t)^m\,\mathrm{d}t,$$

which is in hypergeometric form, and this allows us to write

$$M_{\theta,m} = 2\pi F(-m, 1/2; 1; -\lambda^2).$$

In this case, the first argument $\alpha = -m$ and we can also express this as the degenerate series

$$M_{\theta,m} = 2\pi \sum_{k=0}^{m} (-1)^k \frac{(-m)_k (1/2)_k}{k!^2}\lambda^{2k},$$

and by expressing the Pochhammer terms as binomials and expanding λ we finally obtain

$$M_{\theta,m} = 2\pi \sum_{k=0}^{m} \binom{m}{k}\binom{2k}{k}\left(\frac{b}{2}\right)^{2k}\left(\frac{\sin\phi_s}{\varepsilon + c\cos\phi_s}\right)^{2k}.$$

This allows us to write the following expression for the interaction energy E_{tso} as:

$$E_{tso} = 16\pi^3 a^2 bc\eta_t\eta_s(-AM_3 + BM_6),$$

$$M_n = \frac{1}{(2a)^{2n}(2n-2)!}\sum_{m=0}^{\infty}\left[\frac{(2n+2m-2)!}{(4a)^m m!(n+m-1)!}\right]^2 \sum_{k=0}^{m}\binom{m}{k}\binom{2k}{k}\left(\frac{b}{2}\right)^{2k} M_{\phi,k},$$

$$M_{\phi,k} = \int_0^{\pi} (\varepsilon + c\cos\phi_s)^{2m-2k}\sin^{2k+1}\phi_s (1 - e^2\cos^2\phi_s)^{1/2}\,\mathrm{d}\phi_s,$$

where $e^2 = 1 - (b/c)^2$ is the spheroidal eccentricity. Now we note that from the binomial theorem

$$(\varepsilon + c\cos\phi_s)^{2m-2k} = \varepsilon^{2m-2k}\sum_{\ell=0}^{2m-2k}\binom{2m-2k}{\ell}\left(\frac{c}{\varepsilon}\right)^{\ell}\cos^{\ell}\phi_s,$$

and hence we can write

$$M_{\phi,k} = \varepsilon^{2m-2k} \sum_{\ell=0}^{2m-2k} \binom{2m-2k}{\ell} \left(\frac{c}{\varepsilon}\right)^{\ell} M^{\star}_{\phi,k},$$

$$M^{\star}_{\phi,k} = \int_0^{\pi} \cos^{\ell}\phi_s \sin^{2k+1}\phi_s (1 - e^2\cos^2\phi_s)^{1/2}\,\mathrm{d}\phi_s.$$

As has been previously encountered, $M^{\star}_{\phi,k} = 0$ when ℓ is odd. Therefore these terms can be dropped from the summation by replacing $\ell \to 2\ell$ and hence

$$M_{\phi,k} = \varepsilon^{2m-2k} \sum_{\ell=0}^{m-k} \binom{2m-2k}{2\ell} \left(\frac{c}{\varepsilon}\right)^{2\ell} M^{\star}_{\phi,k},$$

$$M^{\star}_{\phi,k} = \int_0^{\pi} \cos^{2\ell}\phi_s \sin^{2k+1}\phi_s (1 - e^2\cos^2\phi_s)^{1/2}\,\mathrm{d}\phi_s.$$

Now by employing the substitution $t = \cos^2\phi_s$ we deduce that

$$M^{\star}_{\phi,k} = \int_0^1 t^{\ell-1/2}(1-t)^k (1-e^2 t)^{1/2}\,\mathrm{d}t,$$

which again is in the fundamental form for the usual hypergeometric function $F(\alpha, \beta; \gamma; z)$, with $\alpha = -1/2$, $\beta = \ell + 1/2$, $\gamma = k + l + 3/2$ and $z = e^2$, and therefore

$$M^{\star}_{\phi,k} = 2^{2k+1} \frac{(2\ell)!(k+\ell)!k!}{(2k+2\ell+1)!\ell!} F(-1/2, \ell + 1/2; k + \ell + 3/2; e^2).$$

Thus collecting all the terms together for M_n, we obtain

$$\begin{aligned} M_m = \frac{2}{(2a)^{2n}(2n-2)!} \sum_{m=0}^{\infty} \left[\frac{\varepsilon^m (2n+2m-2)!}{(4a)^m m!(n+m-1)!}\right]^2 \\ \times \sum_{k=0}^{m} \binom{m}{k}\binom{2k}{k}\left(\frac{b}{\varepsilon}\right)^{2k} \sum_{\ell=0}^{m-k} \frac{(2m-2k)!(k+\ell)!k!}{(2m-2k-2\ell)!(2k+2\ell+1)!\ell!} \\ \times \left(\frac{c}{\varepsilon}\right)^{2\ell} F(-1/2, \ell+1/2; k+\ell+3/2; e^2), \end{aligned}$$

and as before, we comment that this series expansion converges quickly for spheroids of small eccentricities and when the offset $\varepsilon = 0$ then all the series terms vanish except for $m = 0$ which recovers the axially centered solution.

Appendix J. Interaction with a tilting and offset spheroid

In this appendix, we consider the case of a spheroid which is tilting by an angle ψ and offset from the axis of the nanotube by a distance ε. As in the previous appendix the direction of the offset cannot be assumed without loss of generality. However, as before, the natural direction of offset is in the same direction as that of the tilt and so we assume that the spheroid is tilting around the x-axis and the offset is in the y-direction. Therefore, the parametric form of the spheroidal surface is given by

$$x = b\cos\theta_s \sin\phi_s, \qquad y = \varepsilon + b\sin\theta_s \sin\psi_s \cos\psi - c\cos\phi_s \sin\psi,$$
$$z = c\cos\phi_s \cos\psi + b\sin\theta_s \sin\psi_s \sin\psi,$$

where $-\pi < \theta_s \leqslant \pi$ and $0 \leqslant \phi_s \leqslant \pi$, and therefore

$$\begin{aligned} \rho^2 &= b^2\cos^2\theta_s \sin^2\phi_s + (\varepsilon + b\sin\theta_s \sin\psi_s \cos\psi - c\cos\phi_s \sin\psi)^2 \\ &= \mu + \nu\sin\theta_s - \xi\sin^2\theta_s, \end{aligned}$$

where μ, ν and ξ are given by

$$\mu = b^2 \sin^2\phi_s + (\varepsilon - c\cos\phi_s \sin\psi)^2, \qquad \nu = 2b\sin\phi_s\cos\psi(\varepsilon - c\cos\phi_s\sin\psi),$$
$$\xi = b^2\sin^2\phi_s\sin^2\psi.$$

Expanding ρ^{2m} using the multinomial theorem we have

$$\rho^{2m} = \sum_{p=0}^{m}\sum_{q=0}^{m-p}\frac{(-1)^q m!}{p!q!(m-p-q)!}\mu^{m-p-q}\nu^p\xi^q\sin^{p+2q}\theta_s.$$

Now the θ_s integration is defined as

$$N_{\theta,m} = \sum_{p=0}^{m}\sum_{q=0}^{m-p}\frac{(-1)^q m!}{p!q!(m-p-q)!}\mu^{m-p-q}\nu^p\xi^q\int_{-\pi}^{\pi}\sin^{p+2q}\theta_s\,\mathrm{d}\theta_s,$$

we note that the integral is zero whenever p is odd. Therefore we can replace $p \to 2p$ giving

$$N_{\theta,m} = \sum_{p=0}^{\lfloor m/2\rfloor}\sum_{q=0}^{m-2p}\frac{(-1)^q m!}{(2p)!q!(m-2p-q)!}\mu^{m-2p-q}\nu^{2p}\xi^q\int_{-\pi}^{\pi}\sin^{2p+2q}\theta_s\,\mathrm{d}\theta_s,$$

where $\lfloor x\rfloor$ signifies the largest integer not greater than x and we note that

$$\int_{-\pi}^{\pi}\sin^{2p+2q}\theta_s\,\mathrm{d}\theta_s = \frac{2\pi}{2^{2p+2q}}\binom{2(p+q)}{p+q}.$$

We now expand μ^{m-2p-q} using the binomial theorem giving

$$\mu^{m-2p-q} = \sum_{r=0}^{m-2p-q}\binom{m-2p-q}{r}(b\sin\phi_s)^{2r}(\varepsilon - c\cos\phi_s\sin\psi)^{2m-4p-2q-2r},$$

and continuing in the same way we expand the powers of $(\varepsilon - c\cos\phi_s\sin\psi)$ originating from the μ and ν terms and which we denote by ω, using the binomial theorem thus,

$$\begin{aligned}\omega &= (\varepsilon - c\cos\phi_s\sin\psi)^{2(m-p-q-r)}\\ &= \sum_{s=0}^{2(m-p-q-r)}\binom{2(m-p-q-r)}{s}\varepsilon^{2(m-p-q-r)-s}(c\sin\psi\cos\phi_s)^s,\end{aligned}$$

and we note that the ϕ_s integral terms equal zero when s is odd and therefore we can replace $s \to 2s$ giving an effective $\omega^\star$ of

$$\omega^\star = \sum_{s=0}^{m-p-q-r}\binom{2(m-p-q-r)}{2s}\varepsilon^{2(m-p-q-r-s)}(c\sin\psi\cos\phi_s)^{2s},$$

This allows us to express the interaction energy E_{tto} as

$$E_{tto} = 16\pi^3 a^2 bc\eta_t\eta_s(-AN_3 + BN_6),$$

$$\begin{aligned}N_n = \frac{1}{(2a)^{2n}(2n-2)!}&\sum_{m=0}^{\infty}\left[\frac{\varepsilon^m(2n+2m-2)!}{(4a)^m m!(n+m-1)!}\right]^2\\ &\times\sum_{p=0}^{\lfloor m/2\rfloor}\sum_{q=0}^{m-2p}\frac{(-1)^q m!}{(2p)!q!}\binom{2p+2q}{p+q}\left(\frac{b\cos\psi}{\varepsilon}\right)^{2p}\left(\frac{b\sin\psi}{2\varepsilon}\right)^{2q}\\ &\times\sum_{r=0}^{m-2p-q}\frac{1}{r!(m-2p-q-r)!}\left(\frac{b}{\varepsilon}\right)^{2r}\end{aligned}$$

$$\times \sum_{s=0}^{m-p-q-r} \binom{2(m-p-q-r)}{2s} \left(\frac{c\sin\psi}{\varepsilon}\right)^{2s} N_\phi,$$

$$N_\phi = \int_0^\pi \cos^{2s}\phi_s \sin^{2(p+q+r)+1}\phi_s (1-e^2\cos^2\phi_s)^{1/2}\,\mathrm{d}\phi_s.$$

On making the substitution $t = \cos^2\phi_s$ we obtain

$$N_\phi = \int_0^1 t^{s-1/2}(1-t)^{p+q+r}(1-e^2t)^{1/2}\,\mathrm{d}t,$$

which is similar to those integrals encountered in previous appendices and can be expressed in terms of the usual hypergeometric function as

$$N_\phi = 2^{2(p+q+r)+1}\frac{(2s)!(p+q+r)!(p+q+r+s)!}{s![2(p+q+r+s)+1]!} \times F(-1/2, s+1/2;\ p+q+r+s+3/2;\ e^2).$$

References

[1] Smith B W, Monthioux M and Luzzi D E 1998 Encapsulated C_{60} in carbon nanotubes *Nature* **396** 323–4

[2] Okada S, Saito S and Oshiyama A 2001 Energetics and electronic structures of encapsulated C_{60} in a carbon nanotube *Phys. Rev. Lett.* **86** 3835–8

[3] Hodak M and Girifalco L A 2001 Fullerenes inside carbon nanotubes and multi-walled carbon nanotubes: optimum and maximum sizes *Chem. Phys. Lett.* **350** 405–11

[4] Hodak M and Girifalco L A 2003 Ordered phases of fullerene molecules formed inside carbon nanotubes *Phys. Rev.* B **67** 075419

[5] Hodak M and Girifalco L A 2003 Systems of C_{60} molecules inside (10, 10) and (15, 15) nanotube: a Monte Carlo study *Phys. Rev.* B **68** 085405

[6] Okada S, Otani M and Oshiyama A 2003 Energetics and electronic structure of C_{70}-peapods and one-dimensional chains of C_{70} *New J. Phys.* **5** 122

[7] Troche K S *et al* 2005 Prediction of ordered phases of encapsulated C_{60}, C_{70} and C_{78} inside carbon nanotubes *Nano Lett.* **5** 349–55

[8] Vavro J, Llaguno M C, Satishkumar B C, Luzzi D E and Fischer J E 2002 Electrical and thermal properties of C_{60}-filled single-wall carbon nanotubes *Appl. Phys. Lett.* **80** 1450–2

[9] González Noya E, Srivastava D, Chernozatonskii L A and Menon M 2004 Thermal conductivity of carbon nanotube peapods *Phys. Rev.* B **70** 115416

[10] Okada S, Otani M and Oshiyama A 2003 Electron-state control of carbon nanotubes by space and encapsulated fullerenes *Phys. Rev.* B **67** 205411

[11] Otani M, Okada S and Oshiyama A 2003 Energetics and electronic structures of one-dimensional fullerene chains encapsulated in zigzag nanotubes *Phys. Rev.* B **68** 125424

[12] Khlobystov A N *et al* 2004 Controlled orientaion of ellipsoidal fullerene C_{70} in carbon nanotubes *Appl. Phys. Lett.* **84** 792–4

[13] Cox B J, Thamwattana N and Hill J M 2007 Mechanics of spheroidal fullerenes and carbon nanotubes for drug and gene delivery *Q J. Mech. Appl. Math.* **60** 231–53

[14] Verberck B and Michel K H 2007 Nanotube field and orientational properties of C_{70} molecules in carbon nanotubes *Phys. Rev.* B **75** 045419

[15] Chorro M, Delhey A, Noé L, Monthioux M and Launois P 2007 0rientaion of C_{70} molecules in peapods as a function of the nanotube diameter *Phys. Rev.* B **75** 035416

[16] Hirahara K *et al* 2001 Electron diffraction study of one-dimensional crystals of fullerenes *Phys. Rev.* B **64** 115420

[17] Guan L, Li H, Shi Z, You L and Gu Z 2005 Standing or lying C_{70} s encapsulated in carbon nanotubes with different diameters *Solid State Commun.* **133** 333–6

[18] Cox B J, Thamwattana N and Hill J M 2007 Mechanics of atoms and fullerenes in single-walled carbon nanotubes: I. Acceptance and suction energies *Proc. R. Soc.* A **463** 461–76

[19] Cox B J, Thamwattana N and Hill J M 2007 Mechanics of atoms and fullerenes in single-walled carbon nanotubes: II. Oscillatory behaviour *Proc. R. Soc.* A **463** 477–94

[20] Girifalco L A, Hodak M and Lee R S 2000 Carbon nanotubes, buckyballs, ropes, and a universal graphitic potential *Phys. Rev.* B **62** 13104–10
[21] Nakao K, Kurita N and Fujita M 1994 *Ab initio* molecular-orbital calculation for C_{70} and seven isomers of C_{80} *Phys. Rev.* B **49** 11415–20
[22] Burchnall J L and Chaundy T W 1940 Expansions of Appell's double hypergeometric functions *Q J. Math.* **OS-11** 249–70
[23] Gradshteyn I S and Ryzhik I M 2000 *Table of Integrals, Series, and Products* 6th edn (San Diego, CA: Academic)
[24] Erdélyi A, Magnus W, Oberhettinger F and Tricomi F G 1953 *Higher Transcendental Functions* vol 1 (New York: McGraw-Hill)